



FIELD-WEAKENING AND FATIGUE MANAGEMENT FOR EXPLOSIVE ROBOTICS

S.P. (Sjoerd) Rozendal

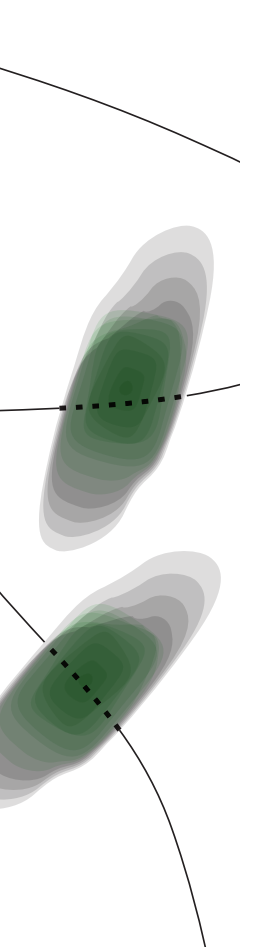
MSC ASSIGNMENT

Committee:

prof. dr. ir. S. Stramigioli dr. ir. W. Roozing dr. ir. J.J. de Jong

October, 2021

071RaM2021 Robotics and Mechatronics EEMCS University of Twente P.O. Box 217 7500 AE Enschede The Netherlands



ii	Field-Weakening and Fatigue Management for Explosive Robotics

Summary

Explosive motions in robotics require both high strength and high velocity actuators. The electrical dynamics of the Permanent Magnet Synchronous Machine (PMSM) motor can be exploited to increase the peak-velocity. An operating method known as field-weakening uses existing current reserves to produce a counteracting magnetic field. This alleviates the voltage constraints, which in turn allows for an increase in peak velocity.

Two field-weakening algorithms were analysed. The Feed-Forward field-weakening algorithm as designed in: 'Enhanced Explosive Motion for Torque Controlled Actuators Through Field Weakening Control' by W. Roozing, was selected. Its only disadvantage is that it strongly depends on the motor parameters. It is evaluated how the performance of this algorithm changes if the motor parameters known in the controller do not fully agree with the actual motor parameters. Results show that the performance of the feed-forward field-weakening strategy quickly degrades if the motor parameters in the controller are not in agreement with the actual motor parameters.

Furthermore, a lot of power is required to perform an explosive motion, hence there is a risk of overheating the motor. A thermal management strategy is presented that has a variable current limit based on the temperature and thermal time constant of the motor. However, in practice the explosive motion is so short that the nominal current over the whole motion stays well below the maximum continuous current.

A jumping leg demo setup is designed in order to apply the field-weakening algorithm to a practical use case. This setup contains a single motor in the hip joint and is constraint such that the leg can only jump up and down along a vertical axis. Simulation results show that the leg can jump about 16 percent higher with the field-weakening control enabled. In practice this improvement was not observed, but the design of the leg can be improved substantially by changing the gear ratio and link length such that field-weakening indeed has an added benefit.

Preface

This report is about field-weakening. It investigates two different field-weakening methods and also presents a fatigue management stratgey. It was written as part of the master thesis of the program Electrical Engineering at the University of Twente.

The assignment has been carried out at the Robotics and Mechatronics group of the University. The assignment was formulated by my daily supervisor dr. ir. W. Roozing. I would like to thank him for his excellent guidance. His critical thinking during the weekly meetings always provided me with useful feedback.

I would also like to thank the technical staff at Robotics and Mechatronics group, in particular ir. S. Smits, for his generous feedback and help for the construction of the robotic leg. Their patience with my many questions and requests for purchases is much appreciated.

Lastly, I would like to thank my family and friends. They have supported and encouraged me all the way through my university life.

Sjoerd Rozendal Enschede,

Contents

1	Intr	ntroduction				
	1.1	Context	1			
	1.2	Goals	1			
	1.3	Document outline	1			
2	Bac	Background				
	2.1	Permanent Magnet Synchronous Motor Electrical Model	3			
		2.1.1 Field Oriented Control	4			
		2.1.2 Clarke Transformation	4			
		2.1.3 Park Transformation	5			
		2.1.4 dq-Motor Model	6			
	2.2	Maximum Torque Per Ampere	7			
	2.3	Field-Weakening	7			
	2.4	Thermal Domain	9			
		2.4.1 Heat Dissipation	9			
		2.4.2 Thermal Capacitance	9			
		2.4.3 Thermal Resistance	9			
3 Analysis			10			
	3.1	PMSM motor types	10			
		3.1.1 IPMSM vs SPMSM	10			
		3.1.2 Inrunner vs Outrunner	11			
	3.2	Field-Weakening	12			
		3.2.1 Model Based method	12			
		3.2.2 Feedback Method	13			
		3.2.3 Proposed Method	14			
3.3 Thermal Modelling and Analysis		Thermal Modelling and Analysis	14			
		3.3.1 Thermal Motor Model	14			
		3.3.2 Fatigue Management	14			
4	Des	gn	16			
4.1 Model overview		Model overview	16			
	4.2	Jumping Leg	17			
5	Res	Results				
5.1 Experiment 1: Deviating motor parameters		Experiment 1: Deviating motor parameters	19			
	5.2	5.2 Experiment 2: Jumping with robotic leg				

		5.2.1	Simulation Results	21	
		5.2.2	Results with Setup	22	
	5.3	Discu	ssion	26	
6	Con	clusio	n and Recommendations	27	
Ał	Abbreviations				
A	App	endix	I	29	
В	App	endix 2	2	30	
Bi	bliog	graphy		31	

1 Introduction

1.1 Context

With the rapid evolution of robotic technology, robots are expected to perform various complicated task that are more and more similar to their biological counterparts. Among these tasks are explosive motions like throwing, kicking or jumping. If a human has to perform such a task he will get fatigued after a while. A human can jump the highest when he just started jumping, but the longer he has to keep jumping the lower the jump height will become as the muscles will become fatigued. If now the robot is given the task to continuously keep jumping it could show the same reduction in jumping performance. Not because the muscles will get fatigued, but because the motor will become so hot that eventually the power going into the motor has to be reduced in order to prevent it from overheating. This reduction in power going into the motor reduces the jumping performance and makes the behavior of the robot more and more comparable to that of a human.

Moreover, explosive motions require both high strength and high velocity actuators. Electric motors are the most common actuator within a robot. This is no surprise as they have a number of advantages over other types of actuators. Electric motors are easy to control, are reliable, have a high power to mass ratio and they can achieve a high level of precision. Therefore, they are very suitable for robotic applications. The electric motor is often paired with a gearbox to get sufficient joint torque. However, this reduces the achievable joint peak-velocity. The electrical dynamics of the Permanent Magnet Synchronous Machine (PMSM) motor can be exploited to increase the peak-velocity. An operating method known as field-weakening uses existing current reserves to produce a counteracting magnetic field. This alleviates the voltage constraints, which in turn allows for an increase in peak velocity.

Explosive motions in robotics require a lot of peak power, but for a short duration of time. The maximum power that is allowed depends largely on the temperature of the windings. Hence, the achievable peak performance is limited by the winding temperature. Furthermore, field-weakening heats up the motor even faster, because in addition to the torque producing current, there now also is a current that weakens the magnetic field.

The possibilities and applications of field-weakening in combination with fatigue management will be explored in this research in order to increase the explosive motion performance of robots.

1.2 Goals

The main goal is to apply field-weakening in an intelligent manner that includes fatigue management of the motor. This is achieved by:

- Researching existing field-weakening methods for torque controlled actuators and analyse the performance of these methods.
- A variable current limit based on the temperature and thermal time constant of the motor, to ensure that the most explosive motion is executed while operating within the temperature limits.
- Designing a prototype jumping robotic leg, to evaluate the field-weakening performance in practice.

1.3 Document outline

The remainder of this report is organised as follows. In Chapter 2, background information is given on how to model and control a PMSM motor. After that, in Chapter 3, the different

types of PMSM motors and field-weakening strategies are analysed. Furthermore, the fatigue management strategy is presented. Then, in Chapter 4, an overview of the controller and plant model is presented and elaborated on. Also, the design of the robotic leg is presented. Finally, in Chapter 5, the performance of the field-weakening algorithm is evaluated with simulation results and real-life results.

2 Background

This chapter contains summarized background information needed to understand how a PMSM motor can be modelled and controlled.

2.1 Permanent Magnet Synchronous Motor Electrical Model

To understand the concept of field-weakening, first a basic understanding of the PMSM motor is required. A typical PMSM motor consists of a stator that houses three windings/coils. These windings can be connected in a star or delta configuration. In a star configuration the three windings are connected to a common point, the neutral. Due to its shape it is also called 'Y' or 'wye'. In a $delta(\Delta)$ configuration there is no neutral point. The star configuration is the most common.

The rotor of a PMSM is made of permanent magnets and a steel shaft that exerts the torque onto the connected devices. The rotor can be designed with different amounts of magnets in the rotor. This is specified as the number of pairs of magnetic poles or also pole-pairs.

A system of three conductors or wires carrying AC voltages is most commonly called a three-phase system. These phases can be labelled A, B and C. In Figure 2.1 the orientation of the magnetic field that is created by the phase currents in the stator is shown for six situations. It can be seen that the magnetic field is rotating in sync with the alternating phase currents that are spatially distributed at 120 degrees apart. The frequency of the rotation is the same as the frequency of the currents. The strength of the magnetic field depends on the magnitudes of the currents. Hence, the speed and torque of the motor can be controlled by accurately controlling the strength and orientation of the magnetic field produced by the currents in the stator.

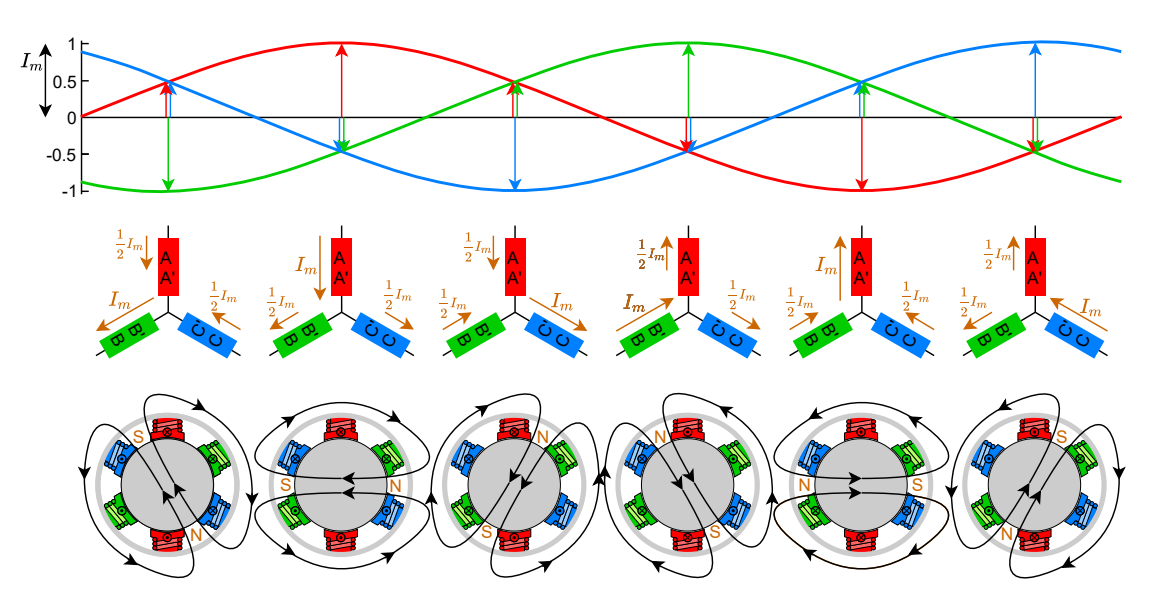


Figure 2.1: The rotating magnetic field inside the stator.

In Figure 2.2 a simplified electrical model of with a three-phase wye-wound stator is shown. Each winding in the stator has an inductance and a resistance.

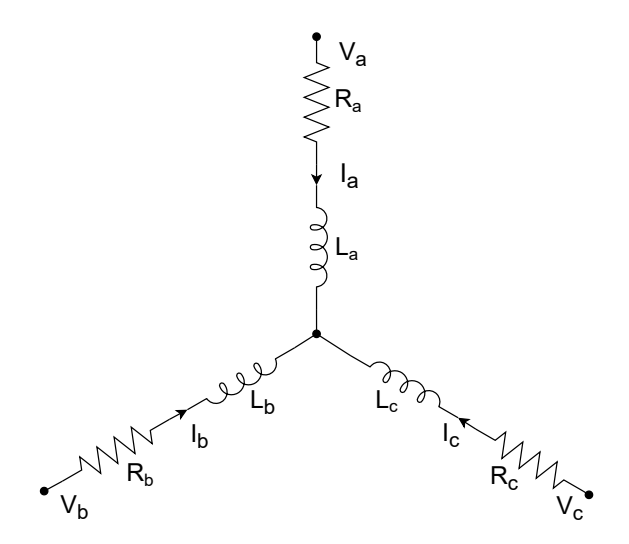


Figure 2.2: Electrical circuit diagram of a PMSM motor.

The voltages across the stator windings are defined by:

$$\begin{bmatrix} V_{\mathbf{a}} \\ V_{\mathbf{b}} \\ V_{\mathbf{c}} \end{bmatrix} = \begin{bmatrix} R_{\mathbf{a}} & 0 & 0 \\ 0 & R_{\mathbf{b}} & 0 \\ 0 & 0 & R_{\mathbf{c}} \end{bmatrix} \begin{bmatrix} i_{\mathbf{a}} \\ i_{\mathbf{b}} \\ i_{\mathbf{c}} \end{bmatrix} + \frac{d}{dt} \begin{bmatrix} \lambda_{\mathbf{a}} \\ \lambda_{\mathbf{b}} \\ \lambda_{\mathbf{c}} \end{bmatrix}$$
(2.1)

$$\begin{bmatrix} \lambda_{a} \\ \lambda_{b} \\ \lambda_{c} \end{bmatrix} = \begin{bmatrix} L_{aa} & L_{ab} & L_{ac} \\ L_{ba} & L_{bb} & L_{bc} \\ L_{ca} & L_{cb} & L_{cc} \end{bmatrix} \begin{bmatrix} i_{a} \\ i_{b} \\ i_{c} \end{bmatrix} + \lambda'_{m} \begin{bmatrix} \sin(\theta_{r}) \\ \sin(\theta_{r} - \frac{2\pi}{3}) \\ \sin(\theta_{r} - \frac{4\pi}{3}) \end{bmatrix}$$
(2.2)

The resistance and inductance is the same for each winding for a balanced motor. Note that the inductance matrix is symmetric. The terms on the diagonal are the self inductances of each phase. The off-diagonal terms are the mutual inductances. λ_m is the permanent magnet flux linkage.

2.1.1 Field Oriented Control

Field Oriented Control (FOC), or also Vector Control, is a method that is used to control the strength and orientation of the magnetic field produced in the stator. The largest torque, due to the permanent magnets, is produced when the magnetic flux of the stator is at 90 degrees with the magnetic flux of the rotor. This is evident from the Lorentz force and the right hand rule for a current carrying wire in a magnetic field. The position of the rotor has to be known in order to align the stator flux with this torque-axis. Without this information the FOC algorithm does not perform optimally.

If you step onto the rotor and rotate with it, you will see two orthogonal components. One component defines the torque (quadrature axis) and the other defines the magnetic flux (direct-axis) of the rotor (see Figure 2.3). In this reference frame the entire control structure becomes linear. Some transformations are required to convert the three phase system to a simple dual phase DC system. These transformations are explained in the next two subsections.

2.1.2 Clarke Transformation

The Clarke transformation, or also $\alpha\beta\gamma$ -transformation, transforms a three phase system to a dual phase system with orthogonal components α and β (see Figure 2.3). α is aligned with the magnetic field axis of phase A. The power invariant transformation is given by Equation 2.3 and

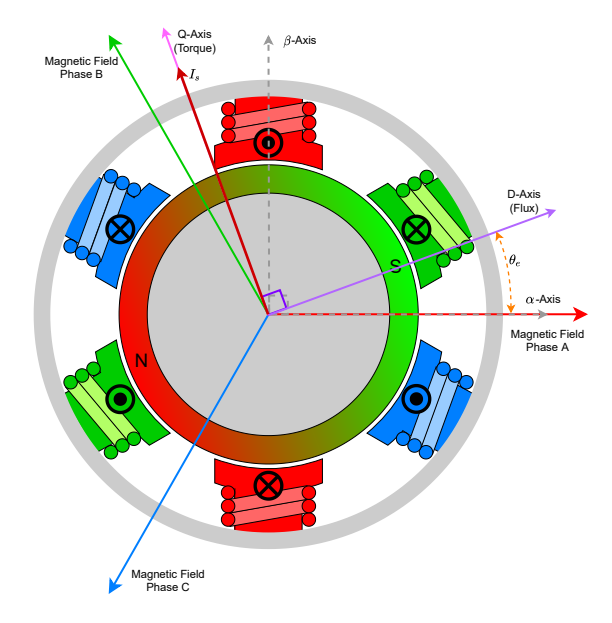


Figure 2.3: The dq-reference frame.

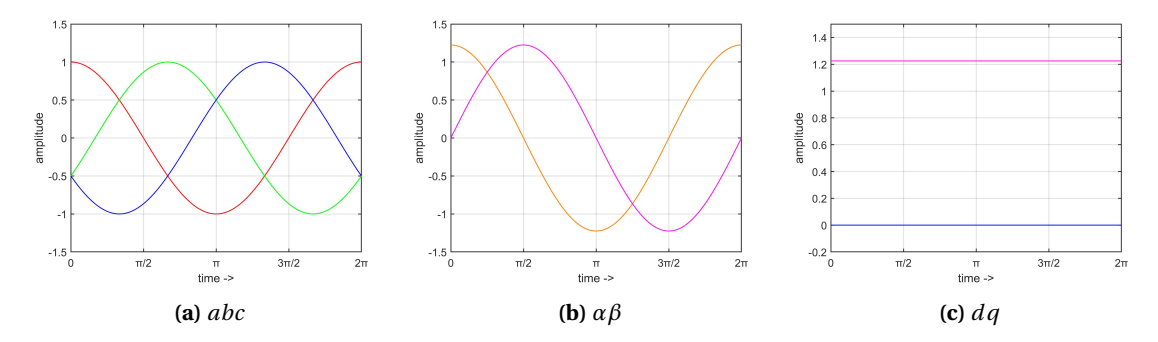


Figure 2.4: Transformation of a three phase system to a dual phase DC system.

its inverse transformation is given by Equation 2.4. Power invariant means that the power in the system before to transformation is equal to the power in the system after the transformation. The Clarke transformation can be applied to the three phase currents as shown in Figure 2.4a. After the Clarke transformation these will look like Figure 2.4b.

$$\begin{bmatrix} f_{\alpha} \\ f_{\beta} \\ f_{\gamma} \end{bmatrix} = \sqrt{\frac{2}{3}} \begin{bmatrix} 1 & -\frac{1}{2} & -\frac{1}{2} \\ 0 & \frac{\sqrt{3}}{2} & -\frac{\sqrt{3}}{2} \\ \frac{1}{\sqrt{2}} & \frac{1}{\sqrt{2}} & \frac{1}{\sqrt{2}} \end{bmatrix} \begin{bmatrix} f_{a} \\ f_{b} \\ f_{c} \end{bmatrix}$$
(2.3)

$$\begin{bmatrix} f_a \\ f_b \\ f_c \end{bmatrix} = \sqrt{\frac{2}{3}} \begin{bmatrix} 1 & 0 & \frac{1}{\sqrt{2}} \\ -\frac{1}{2} & \frac{\sqrt{3}}{2} & \frac{1}{\sqrt{2}} \\ -\frac{1}{2} & -\frac{\sqrt{3}}{2} & \frac{1}{\sqrt{2}} \end{bmatrix} \begin{bmatrix} f_a \\ f_{\beta} \\ f_{\gamma} \end{bmatrix}$$
(2.4)

2.1.3 Park Transformation

The Park transformation, or also dq0-transformation, is a transformation from a stationary frame, the $\alpha\beta$ -frame, to a rotating frame, the dq-frame, (see Figure 2.3). This transformation

shifts the frequency spectrum of the signal with the frequency of that signal, such that the signal now appears as a DC signal. The transformation is given by:

$$\begin{bmatrix} f_q \\ f_d \\ f_0 \end{bmatrix} = \begin{bmatrix} \cos(\theta_e) & \sin(\theta_e) & 0 \\ -\sin(\theta_e) & \cos(\theta_e) & 0 \\ 0 & 0 & 1 \end{bmatrix} \begin{bmatrix} f_\alpha \\ f_\beta \\ f_\gamma \end{bmatrix}, \tag{2.5}$$

where θ_e is the electrical angle between the magnetic field axis of phase A and the flux-axis of the rotor(see Figure 2.3). For the simple case where the rotor has one pole-pair, the electrical angle is equal to the mechanical angle of the rotor. When the rotor has more pole-pairs the electrical angle can be calculated with:

$$\theta_e = p \cdot \theta_m, \tag{2.6}$$

where p is the number of pole-pairs. The electrical angular rotor velocity ω_e is also p times the mechanical rotor velocity ω_m .

After the Park transformation the $\alpha\beta$ -signals will transform to two DC signals (see Figure 2.4c)

2.1.4 dq-Motor Model

The voltages, current, resistances and inductances can all be transformed to the dq-reference frame using the Clarke & Park transformations. The electrical schematic of the motor in the dq-frame is shown in Figure 2.5. The resulting voltages v_q and v_d are given in Equation 2.7.

$$v_{q} = Ri_{q} + L_{q} \frac{di_{q}}{dt} + \omega_{e} L_{d} i_{d} + \omega_{e} \lambda_{m}$$

$$v_{d} = Ri_{d} + L_{d} \frac{di_{d}}{dt} - \omega_{e} L_{q} i_{q}$$
(2.7)

 $v_{\rm q}$, $v_{\rm d}$ are the voltages in the q- (quadrature) axis and d- (direct) axis. $i_{\rm q}$, $i_{\rm d}$ are the currents in the same axis. $L_{\rm q}$, $L_{\rm d}$ represent the q- and d-axis inductances, R is the winding resistance and $\lambda_{\rm m}$ denotes the permanent magnet flux linkage and $\omega_{\rm e}$ is the electrical angular rotor velocity.

The motor torque T_{em} is can be calculated with:

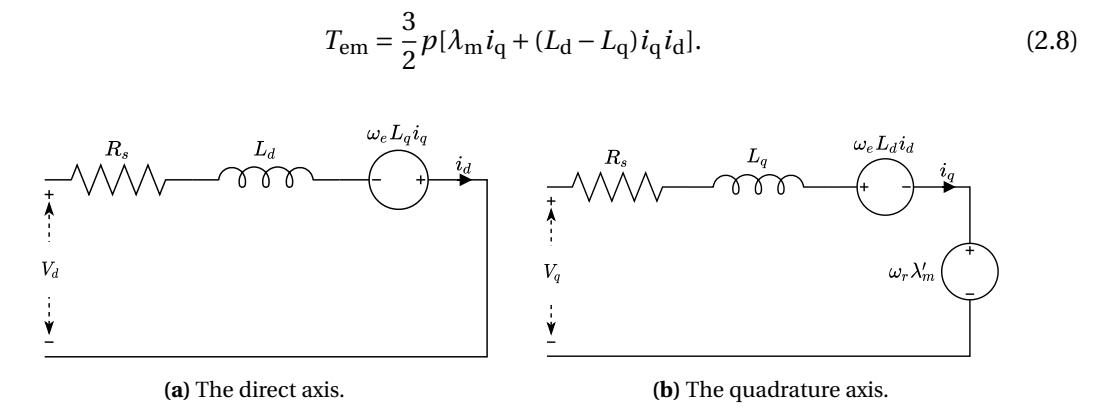


Figure 2.5: dq-model of a PMSM motor.

2.2 Maximum Torque Per Ampere

Maximum Torque Per Ampere (MTPA) is a high-efficient control strategy that maximises the generated torque per Ampere. In other words, it keeps the required current to produce a certain torque to a minimum such that copper losses are minimised. This mode is used when operating the motor within the voltage and current constraints. These are shown in Equation 2.9 and 2.10). The current limit is determined by factors like: thermal dissipation capabilities of the motor, cooling methods and available output current of the inverter. The voltage limit is determined by the DC source voltage, $v_{max} = v_{dc}/\sqrt{3}$.

$$i_{\rm d}^2 + i_{\rm q}^2 \le i_{\rm max}^2$$
 (2.9)

$$v_{\rm d}^2 + v_{\rm q}^2 \le v_{\rm max}^2 \tag{2.10}$$

From Equation 2.8 it can be seen that a certain torque can be reached by multiple combinations of $i_{\rm d}$ and $i_{\rm q}$. It is common to express $i_{\rm d}$ as a function of $i_{\rm q}$ (see Equation 2.11) in order to find the current references where the magnitude of the stator current is smallest (Sue and Pan, 2008).

$$i_{\rm d} = \frac{\lambda_{\rm m}}{2(L_{\rm d} - L_{\rm q})} - \sqrt{\frac{\lambda_{\rm m}^2}{4(L_{\rm d} - L_{\rm q})^2} + i_{\rm q}^2}$$
 (2.11)

The maximum base speed that can be reached with the MTPA control strategy is limited by the back-EMF voltage produced by the motor. The back-EMF voltage is found by setting the torque and thus also the currents to zero. That leaves a single steady state term in Equation 2.7 which is the back-EMF.

$$v_{\rm EMF} = \omega_{\rm e} \lambda_{\rm m} \tag{2.12}$$

If a frictionless drive is considered, the maximum speed that can be reached is when the back-EMF voltage is equal to the maximum phase voltage. Hence, this can be calculated by:

$$\omega_{\rm m}^{\rm max} = \frac{\nu_{\rm max}}{p\lambda_{\rm m}}. (2.13)$$

2.3 Field-Weakening

A negative voltage can be induced in the quadrature axis current loop by applying a negative $i_{\rm d}$ current (see the steady state equations 2.14 and 2.15 for the circuit in Figure 2.5). This alleviates the voltage constraints (Equation 2.10) such that higher speeds can be reached at the expense of larger currents. The negative $i_{\rm d}$ current produces an electromagnetic flux that opposes the permanent magnet flux, thus reducing the total magnetic flux. This process is called field-weakening, or flux-weakening.

$$v_{\rm q} = Ri_{\rm q} + \omega_{\rm e}L_{\rm d}i_{\rm d} + \omega_{\rm e}\lambda_{\rm m} \tag{2.14}$$

$$v_{\rm d} = Ri_{\rm d} - \omega_{\rm e} L_{\rm g} i_{\rm g} \tag{2.15}$$

The voltage limit ellipses can be obtained be substituting the steady state equations 2.14 and 2.15 into Equation 2.10. This results in Equation 2.16.

$$(R_{s}i_{d} - \omega_{e}L_{q}i_{q})^{2} + (R_{s}i_{q} + \omega_{e}L_{d}i_{d} + \omega_{e}\lambda_{m})^{2} = \nu_{max}^{2}$$
(2.16)

Solving Equation 2.16 for ω_e gives two solutions corresponding to a positive or negative angular velocity.

Figure 2.6 shows these voltage limits for various motor velocities, plotted in the $i_{\rm d}$, $i_{\rm q}$ plane. The figure has been created with parameters from the Maxon EC60 Flat motor in Appendix A. The current limit is set to 15 Ampere and is depicted as the magenta colored circle. The maximum theoretical speed without field-weakening is calculated with Equation 2.13 and is about 396 [rad/s]. In the figure this is represented by the voltage ellipse that goes through the origin. In a practice this speed will be lower, since a non-zero torque is required to overcome the frictional forces in order to maintain a certain velocity.

$$\omega_{m}^{FW} = \frac{\omega_{e}}{p} = \frac{1}{p} \sqrt{\frac{V_{max}^{2} - R^{2} I_{max}^{2}}{\lambda_{m} - L_{d} I_{max}}}$$
(2.17)

The maximum speed that can be achieved with field-weakening can be determined by solving Equation 2.16 for $\omega_{\rm e}$ with $i_{\rm q}=0$ and $i_{\rm d}=-I_{\rm max}$. With the parameters of the motor as given in Appendix A, the maximum speed with field-weakening is 672 [rad/s]. This is an increase of almost 70 percent compared to the maximum speed of the motor without field-weakening. In practice the maximum speed with field-weakening is much lower, since, once again, $i_{\rm q}$ has to be non-zero in order to maintain a certain velocity. Furthermore, other non-linear effects start to appear. For example, the direction of the electromagnetic field created by the windings has to be changed at such a high rate that it cannot build up to its full strength (Maxon Motor, 2021). Experimental results in the work presented in Roozing et al. (2018) still show that a significant improvement of the output speed is achieved of up to 33%.

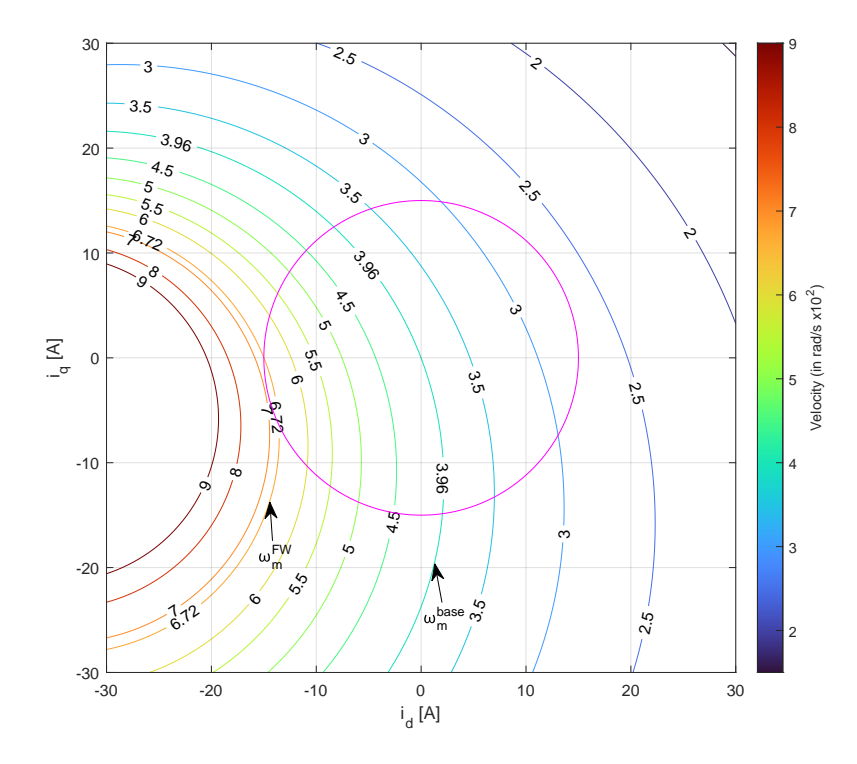


Figure 2.6: Voltage limits for various positive velocities. The rainbow colored arcs depict the voltage limit ellipses for various velocities. The magenta line indicates the current limit circle. ω_m^{base} is the maximum theoretical speed that can be reached without field-weakening. ω_m^{FW} is the maximum theoretical speed that can be reached with field-weakening

2.4 Thermal Domain

The thermal domain is modelled with entropy. Its elements are presented in Breedveld (2001) and are summarized in the next subsections.

The thermal domain can be modelled with entropy $(\frac{dS}{dt})$ as the flow variable and temperature (T), in Kelvin, as the effort variable.

$$\frac{dQ}{dt} = T\frac{dS}{dt} \tag{2.18}$$

 $\frac{dQ}{dt}$ is the heat flow which is equivalent to power. Entropy is considered as a state variable, however it cannot be expected to obey the global conservation principle, since global conservation of entropy does not exist. In other words, heat cannot go from a storage element with a low temperature to a storage element with a higher temperature without adding energy to the system.

2.4.1 Heat Dissipation

Two concepts can be described with entropy. The first is the irreversible and global increase of entropy in a system. The 'R'-element in most domains is the resistive element that represents dissipation of heat. It is responsible for this irreversible increase in entropy. The relationship between the electrical domain and thermal domains is defined as:

$$P_{in} = u \cdot i = \frac{dQ}{dt} = T \frac{dS_{irr}}{dt} = P_{thermal}$$
 (2.19)

2.4.2 Thermal Capacitance

The second concept is the reversible storage of entropy which can be represented by a thermal capacitor. This C-element behaves slightly different than the C-element from other domains. It is defined as:

$$T = T_0 e^{\frac{S - S_0}{C}},\tag{2.20}$$

where T_0 is the ambient room temperature, S_0 the initial entropy stored in the capacitor and C is the heat capacitance.

2.4.3 Thermal Resistance

A system can have multiple components that have different temperatures. Therefore, these components may also conduct heat between one another. This heat conductor can be modelled as an 'RS' element with an input thermal power port and an output thermal power port. The element is described by the following equations:

$$\frac{dS_{in}}{dt} = \frac{1}{R} \frac{T_{in} - T_{out}}{T_{in}} \tag{2.21}$$

$$\frac{dS_{out}}{dt} = \frac{1}{R} \frac{T_{in} - T_{out}}{T_{out}},\tag{2.22}$$

where R is the thermal resistance in Kelvin/Watt.

3 Analysis

Multiple PMSM motor types are researched. A thermal management strategy is presented and two different field-weakening methods are analysed.

3.1 PMSM motor types

Multiple types of a PMSM motor exist. The main differences are how the permanent magnets are mounted, and if the rotor is on the inside or outside of the stator windings. These types are discussed below.

3.1.1 IPMSM vs SPMSM

The main distinction of a PMSM is made in how the permanent magnets are mounted on the rotor. It can be a Surface Permanent-Magnet Synchronous Machine (SPMSM) or an Interior Permanent-Magnet Synchronous Machine (IPMSM), see Figure 3.1. The equations as described in Section 2.1.4 can be used for both types of PMSM motor. The difference between them is in the way they can produce a torque.

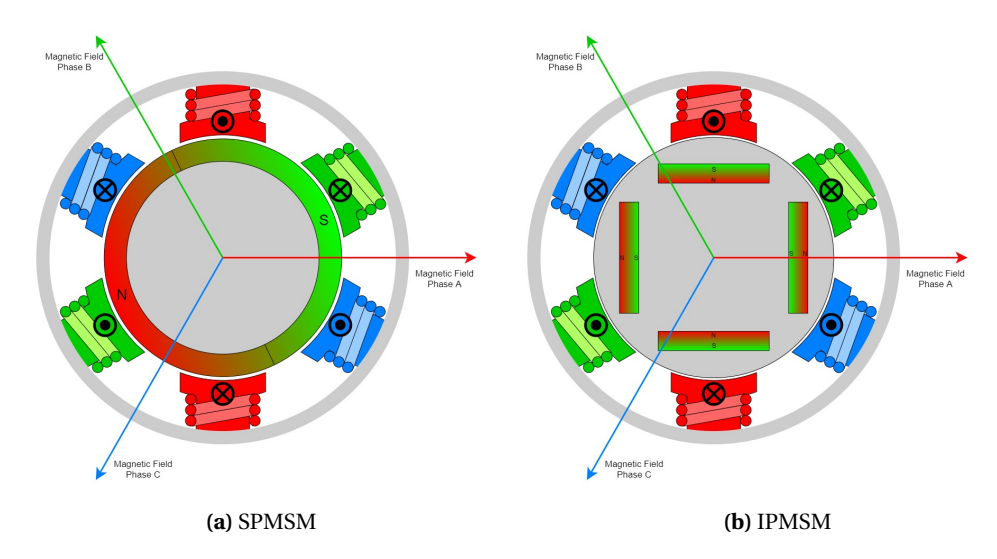


Figure 3.1: Examples of magnet mounting for a SPMSM and IPMSM

The magnetic field lines, produced by the stator of an IPMSM, have different material paths through the rotor depending on the position of the rotor. This means that it also experiences different resistances depending on this path. Therefore, an IPMSM can generate a reluctance torque. In dq-motor model this difference expresses itself as a difference in the q-axis and d-axis inductances ($L_d \neq L_q$). A given torque setpoint can be achieved by multiple combinations of q- and d-axis currents, see Equation 2.8. Finding the MTPA point is not straightforward and in most cases a look-up table is used that contains the optimal q- and d-axis currents for a certain operating point. An IPMSM is mechanically more robust compared to a SPMSM, since the magnets are inside the rotor and not glued to the surface. The IPMSM also is more efficient as it can use both a reluctance torque and a magnetic torque.

Finding the MTPA point for a SPMSM is easier. The magnetic field lines do not have different material paths through the rotor. Hence, the q-axis and d-axis inductances are equal ($L_d = L_q$).

Therefore, the SPMSM cannot produce a reluctance torque and Equation 2.8 can be simplified to:

$$T_{em} = \frac{3}{2}p[\lambda_m i_q] \tag{3.1}$$

Now the q-axis current is directly related to a given torque setpoint. Note that i_d does not produce any torque and thus is set to zero for normal MTPA control. Modelling and controlling a SPMSM is easier compared to an IPMSM. Also, the proposed field-weakening algorithm in Section 3.2.3 only works for an SPMSM (Roozing et al., 2018).

3.1.2 Inrunner vs Outrunner

An electric motor consists of a stator and a rotor. Most commonly the rotor is on the inside of the stator windings. This is a so-called inrunner motor. However, it is also possible to have the permanent magnets attached to a ring on the outside of the stator windings. This is a so-called outrunner.

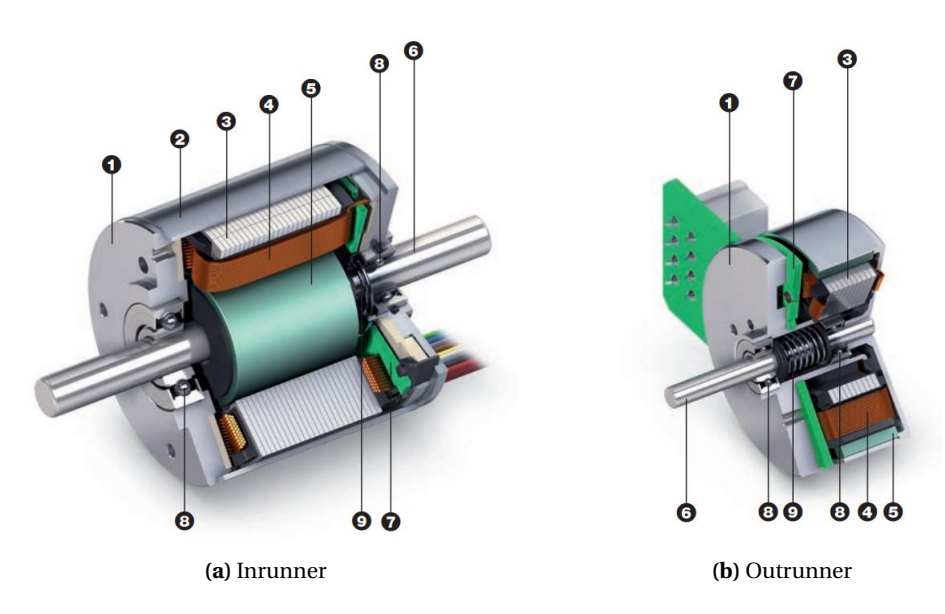


Figure 3.2: Example of an inrunner and outrunner. With (1) Flange, (2) Housing, (3) Laminated steel stack, (4) Winding, (5) Permanent Magnet, (6) Shaft, (7) Print with Hall Sensors, (8) Ball bearing, (9) Spring Bearing (Maxon Motor, 2014)

There are several benefits to having the rotor on the outside of the windings. Firstly, the air gap surface is quite a bit larger. Therefore, the surface area through which the electromagnetic field lines pass is much larger, resulting in a higher torque. Secondly, the electromagnetic force is generated further from the centre of rotation. Hence, the arm of the force is larger, resulting again in a higher torque. Therefore, an outrunner motor can generate higher torque levels than an inrunner motor within the same build volume.

By design an outrunner requires a larger rotor in order to house the stator. Therefore, the outrunner has a higher inertia compared to an inrunner. This is not beneficial since more mass needs to be accelerated in order to perform the explosive motion. However, the larger rotor inertia also helps to dampen the torque ripple. Especially at low speeds it helps to provide a smooth and more stable operation.

The model based field-weakening algorithm is chosen in Section 3.2. This field-weakening method only works for a SPMSM motor. Furthermore, an IPMSM requires a full characterization in order to create the look-up table. The look-up table has a similar disadvantage as the

model based field-weakening strategy. It also does not include changes in motor parameters due to temperature changes. Therefore, the SPMSM motor is used for this research.

The outrunner motor has a higher torque density in a similar package size compared to an inrunner. Hence, the outrunner motor is the best suited motor for a robotic application where the weight and volume should be as low and small as possible. The lighter the robot the more efficient as less mass has to be moved.

3.2 Field-Weakening

A field-weakening strategy for torque controlled robotic applications can be implemented in two ways. It can be done with a model-based feed-forward controller (Roozing et al., 2018), or it can be done with a feedback controller (Mohammadnia et al., 2019). These methods and their advantages are briefly described in the following subsections. Finally, the author presents an improvement of the model based method.

3.2.1 Model Based method

The model based feed-forward control method is presented in Roozing et al. (2018). It is continuous in speed and operates using only a torque reference. The strategy can only be applied to an SPMSM motor as no closed form solutions exist for IPMSMs. The strategy consists of four operating modes. These modes are based on the system dynamics and the voltage and current constraints.

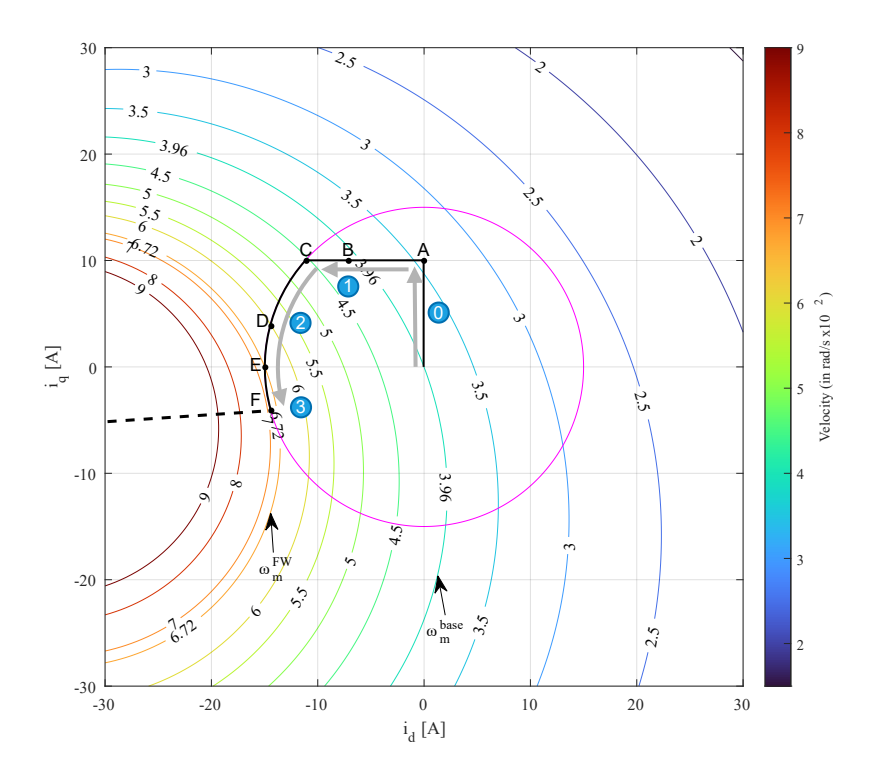


Figure 3.3: d-q operating points for the four operating modes. The gray arrows depicted the movement of each mode while the motor speeds up. The magenta circle depicts the current limit.

In Figure 3.3 the operating points in the d-q plane are shown. The rainbow colored arcs depict the voltage limits for various motor velocities. The magenta line indicates the current limit circle. An explosive motion starts out at stand still or a very low velocity. Hence, the control starts in mode 0, the MTPA mode (see Section 2.2).

CHAPTER 3. ANALYSIS 13

• **Mode 0:** MTPA mode (Point A). The required torque can be achieved without exceeding the current or voltage limit.

- **Mode 1:** Voltage limited mode (from Point A to C). The requested torque and therefore i_q current can be maintained by applying a negative i_d current in order to reduce the back-emf of the motor. The norm of the current vector is still smaller than the current limit
- Mode 2: Voltage and current limited mode (from Point C to E). The norm of the current vector is equal to the current limit. The only way to go faster is by applying an even larger negative i_d current and reducing the back-emf even more. However, the current limit can not be exceeded. Therefore, the magnitude of i_q and thus the produced torque is decreased in order to stay within the current limits.
- **Mode 3:** No overlap mode (the dashed line from point F). The motor is being driven externally and both the voltage and current constraint cannot be satisfied. In this case the magnitude of the voltage vector is minimized.

In modes 1 and 2 the amount of i_d current is computed based on the system dynamics and the voltage and current constraints. The i_d current on its own does not contribute to any torque production by itself. It alleviates the voltage limit and produces some additional heat. Hence, the amount of i_d current should just be enough such that either, in mode 1, the i_q current can be maintained or, in mode 2, the i_q current that is sacrificed is as little as possible.

The equations to calculate i_q and i_d for each mode strongly depend on the motor parameters. This is also the largest disadvantage of this method. It is crucial to accurately measure the motor parameters in order for the strategy to work optimally, as will be shown in Section 5.1. Furthermore, the motor parameters are subject to change while operating the motor. For instance, the motor heats up while in use, changing the winding resistance and also the permanent magnet flux. An increase of 50°C in winding temperature results in an increase of 20% in winding resistance R as calculated by Equation 3.2 with the temperature coefficient for copper $\alpha_{Cu} = 0.0039$ [°C⁻¹] and T the current winding temperature.

$$R(T) = R_{25^{\circ}C} \cdot (1 + \alpha_{Cu}(T - 25^{\circ}C))$$
(3.2)

This is not the only thing that changes in the motor due to a temperature change of 50°C. According to the product pages of Maxon Motor (2021) the permanent magnets are weakened by 1 to 10% depending on the permanent magnet material. Therefore, the largest consequence of the higher temperature is that more current is required to produce the same amount of torque. The change in permanent magnet flux can be calculated with Equation 3.3 with T the permanent magnet temperature. α_{Magnet} typically is -0.0012 [°C⁻¹] for a neodymium magnet (Montone, 2020), but strongly depends on the magnet quality.

$$\lambda_m(T) = \lambda_{m \ 25^{\circ}C} \cdot (1 + \alpha_{Magnet}(T - 25^{\circ}C)) \tag{3.3}$$

The same product pages also state that at higher rotor speeds, the current in the stator cannot fully develop during the short commutation intervals. Therefore, the apparent torque is lower as the motor's behaviour does not follow the ideal linear speed-torque gradient anymore. Hence, at higher rotor speeds the calculated setpoints using the ideal linear model might not match the actual situation. This will reduce the top speed of the motor. It is assumed that the speed at which this happens are not reached.

3.2.2 Feedback Method

The feedback field-weakening strategy is presented in Mohammadnia et al. (2019). This method does not require the measurement of the velocity of the motor for its calculations. It

uses the commanded voltages of the current controller v_q*,v_d* and the measured currents i_q^* . This control scheme has three modes of operation.

- Mode 0: MTPA mode. The required torque can be achieved without exceeding the current or voltage limit.
- Mode 1 Voltage limited mode. Field-weakening is engaged at the point where the commanded voltage vector has become larger than the maximum voltage. The error is defined as the difference between the commanded voltage vector and the maximum voltage. The required negative i_d current is regulated by a conventional PI-controller that acts on the voltage error.
- Mode 2 Voltage and current limited mode. Mode 2 is engaged when both the voltage and current are saturated. The direct current needs to become even more negative. The same voltage error is used in this mode. However, now a PI-controller with different gains is used. Also, the quadrature current is reduced correspondingly such that the current limit is respected. This continues until a steady speed is reached.

The commanded voltages and measured currents in the dq-frame are, for most motor controllers, very noisy. This noise directly enters the PI-controllers resulting in reference voltages with large noise levels. These in turn generate large spikes in the currents that enter the motor. This effect is especially poor in mode 2 if the magnitude of the commanded i_d^* current reaches the current limit, setting the i_q current to zero. Figure 7b of the paper presented by (Mohammadnia et al., 2019) shows that the quadrature current has swings of more than 5 amperes. These swings could make the control loop unstable and will also generate large I^2R losses.

3.2.3 Proposed Method

As explained in the previous subsection the feedback method has some caveats that make it less robust as the model based method. However, the performance of the model-based feedforward method strongly depends on the motor parameters. These parameters are subject to change mainly due to temperature changes in the motor. Hence, assuming that the motor parameters can be obtained accurately, the only addition is to measure the temperature of the windings of the motor during operation. The motor parameters known in the field-weakening controller can then be adjusted using the measured temperature. A temperature sensor in the motor has the added benefit that it can also be used for the thermal management of the motor. These temperature readings are more accurate compared to estimating the motor temperature by measuring the motors winding resistance.

3.3 Thermal Modelling and Analysis

Field weakening requires to operate the motor above the nominal current limits. Hence, there is a significant risk of overheating the motor. In the worst-case scenario the windings can be damaged or demagnetisation of the permanent magnets can occur. Therefore, a control solution is required that prevents the motor from overheating.

3.3.1 Thermal Motor Model

With all the components mentioned in Section 2.4 the thermal model for a PMSM motor can be constructed, see Figure 3.4. Heat is dissipated in the windings. This creates an irreversible increase of entropy. This entropy is stored in the thermal capacitance of the windings. The windings are connected to the housing, hence heat is conducted from the windings to the housing. Finally, this heat is conducted/radiated to the environment.

3.3.2 Fatigue Management

Fatigue management can be done by looking at the thermal time constant of the electric motor. When the motor is operating above the nominal current limit, an explosive action can only

CHAPTER 3. ANALYSIS 15

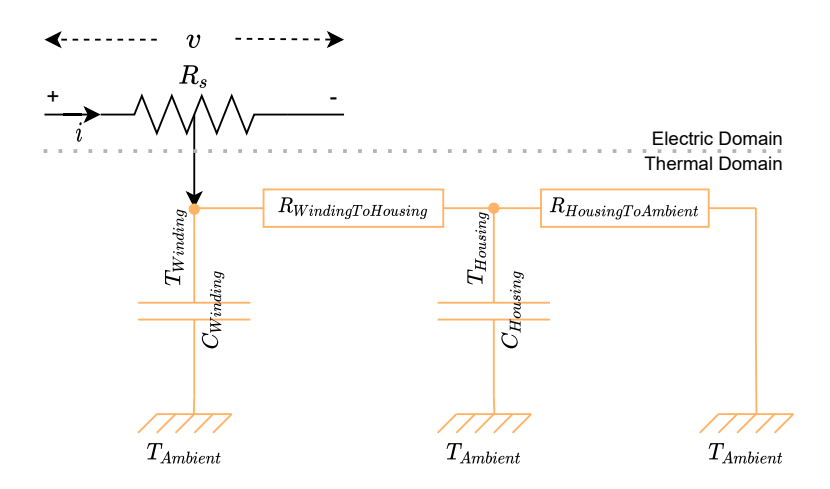


Figure 3.4: The thermal model of a PMSM motor.

take so long before the motor overheats. Therefore, the maximum allowable current can be set according to the temperature of the motor at that moment. It will drop the higher the temperature of the motor becomes. It can be thought of as a variable current limit based on the current temperature of the motor and the thermal time constant of the motor.

The windings are the critical part of the motor as these heat up due to the electrical current. The worst-case scenario would be if the current going trough the windings is the maximum allowable current and that there is no heat flowing to the environment. This assumption can be made, since the duration of the explosive motion is much shorter than the thermal time constant of the motor (9.19 seconds in the of the motor in Appendix A). Therefore, the thermal domain part of the schematic in Figure 3.4 can be simplified to only $C_{Winding}$. The power flowing from the electrical domain into the thermal domain is constant, since the current going trough the resistor is the maximum allowable current. Therefore, the temperature will increase linearly over time. With Equation 3.4 the time in which the windings reach the temperature limit can be calculated.

$$T_{max} - T_0 = \frac{I_{max}^2 R_s}{C_{Winding}} (t_{end} - t_{start})$$
(3.4)

This relation can also be inverted. A time can be set at which it is allowed for the windings to reach the maximum temperature. Given the current temperature of the motor, this can then be used to calculate the current limit.

$$I_{lim} = \sqrt{\frac{(T_{max} - T_0)C_{Winding}}{R_s(t_{end} - t_{start})}}$$
(3.5)

For example, when the starting temperature is 25°C, the maximum temperature is 100°C, $t_{end} - t_{start}$ is the thermal time constant of 9.19 seconds, the phase resistance R_s of 0.293/2 and thermal winding capacitance of 10.9, it would result in a current limit of 24.6 amperes. The resulting current limit is reduced to 14.2 amperes if the starting temperature is already at 75 °C.

The behaviour of the robot becomes comparable to that of a human. If a human has to perform explosive motions like jumping, throwing or kicking, he will also get fatigued after a while. The human can jump the highest at the start, but the longer he has to keep jumping the lower the jump height will become as the muscles will become fatigued. This will be the same for the robot. If it just started jumping the motor is close to room temperature, but after a while the motor will become hot. The maximum allowable current calculated with Equation 3.5 will become lower as the temperature gets higher.

4 Design

4.1 Model overview

Matlab in combination with Simulink is used to model the PMSM motor and to tune the control algorithms before these are tried with an actual motor. The added benefit of using this program is that the control algorithms can directly be used to control an actual motor controller with an additional package called: "Simulink Desktop Real Time".

Simulink Desktop Real Time provides a real-time kernel that can execute Simulink models on a computer running Windows. The control algorithms are first simulated within Simulink with a model of the plant. Then, the same algorithms are executed on the real-time kernel from where it can control a physical device via UART or another communication protocol. This drastically reduced the time needed for programming and also allowed easy tuning of the control algorithm without the need to reprogram anything. Depending on the complexity of the model and the I/O blocks used a control loop frequency up to 1kHz can be achieved.

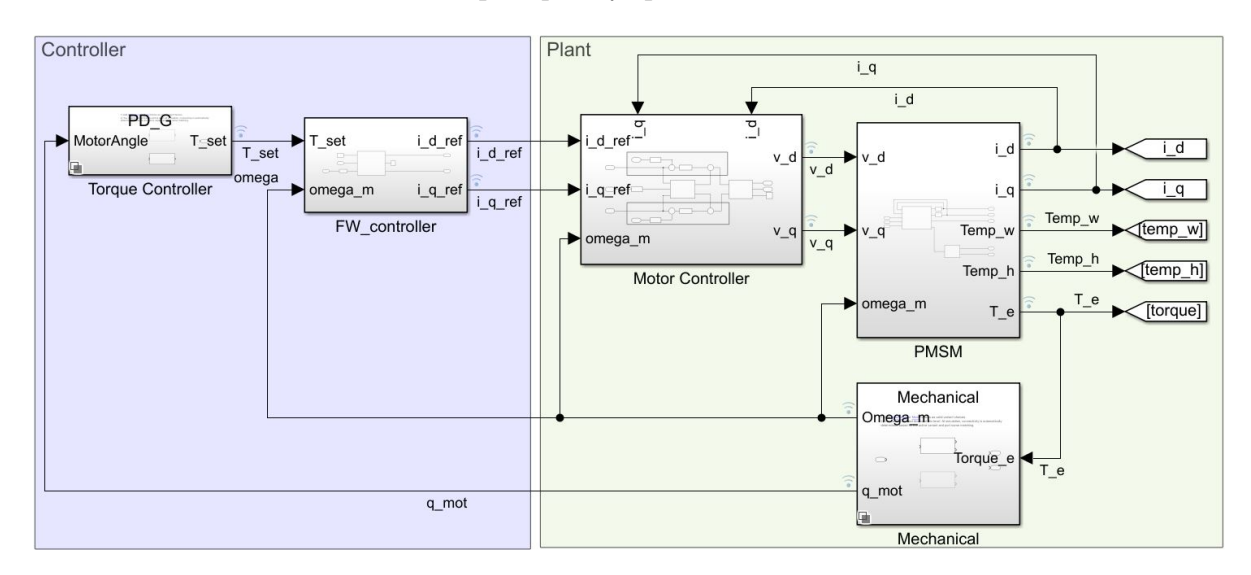


Figure 4.1: The full model as implemented in Simulink.

The Simulink model of the controllers, SPMSM, and the mechanical model is shown in Figure 4.1. The torque controller block has a PD-controller that controls the torque required to keep the motor at a certain position. The FW_controller block contains the field-weakening algorithm as described in detail in Roozing et al. (2018). The motor controller block contains a model of how the currents are regulated on an actual motor controller board. The PMSM block contains the model of the electrical motor as described in Section 2.1.4. The mechanical block is either a simple inertia and some damping for experiment 1, or it contains the multibody dynamics of the leg as presented in Section 4.2 for experiment 2.

The Simulink model of the motor controller is shown in Figure 4.2. The block receives the current setpoints. The PI-controllers regulate the direct and quadrature voltages in such a way that the error between the reference currents and the measured currents goes to zero. The PI-controllers run at a frequency of 10kHz. The feed-forward block calculates the steady stage voltages needed to achieve the reference currents in the motor according to Equations 2.14 and 2.15. In real life there are also some voltage constraint that need to be adhered to. In the model the DQ Limiter block ensures that the voltages stay within the voltage constraints.

CHAPTER 4. DESIGN 17

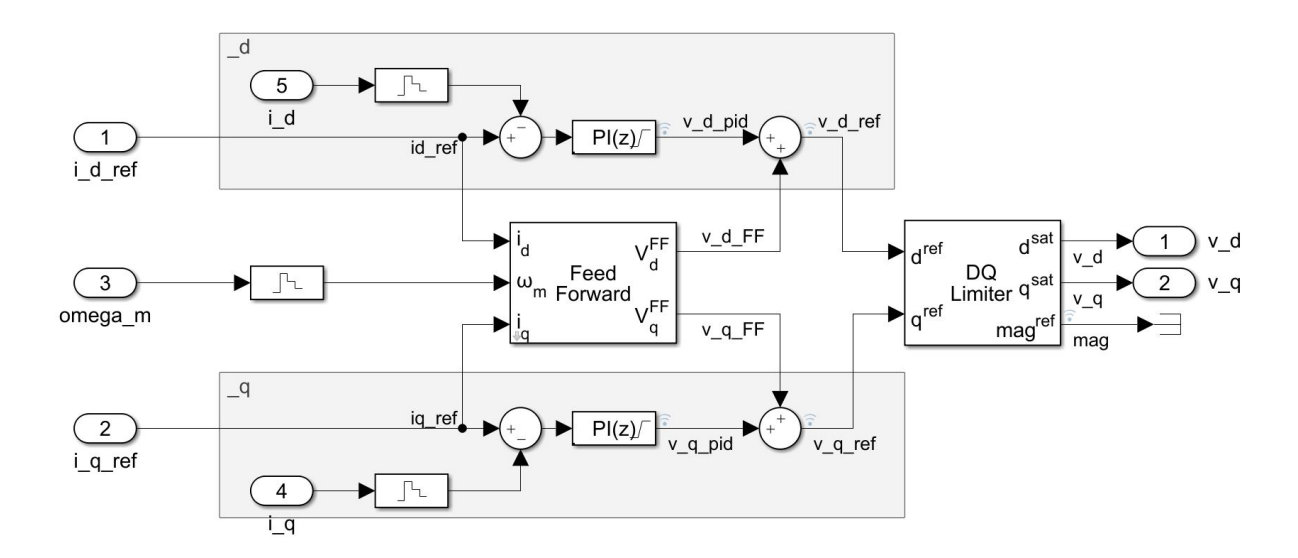


Figure 4.2: The model of the motor controller.

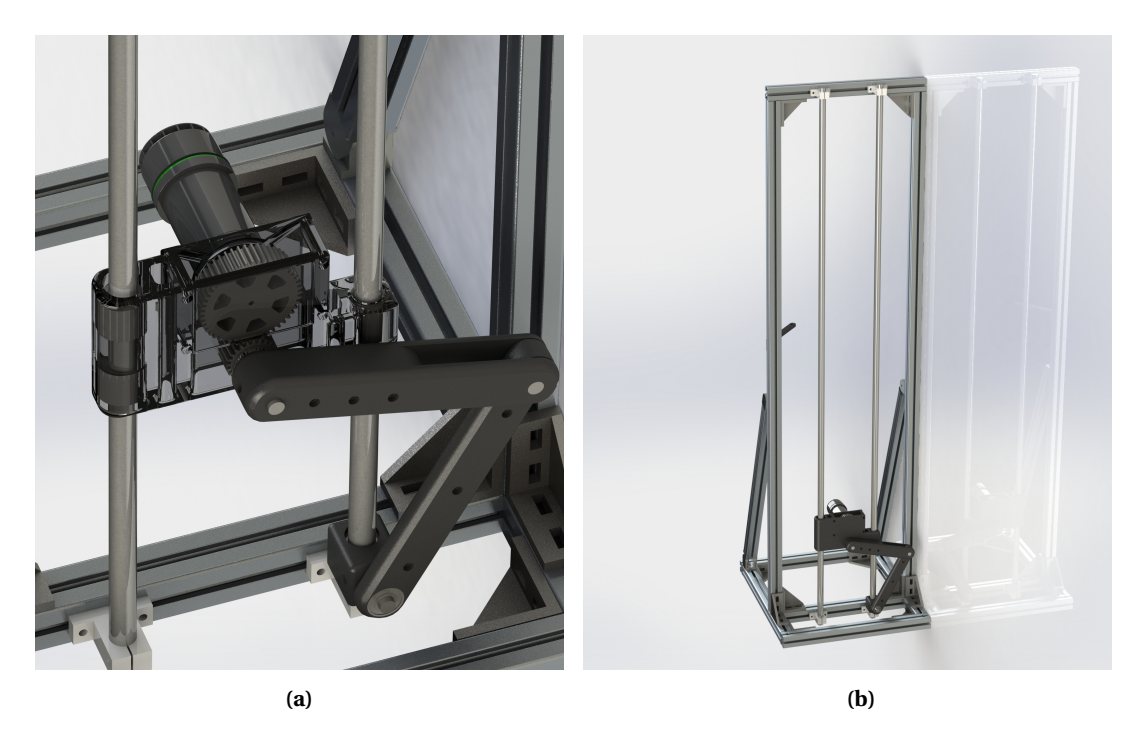
The thermal management strategy as presented in Section 3.3.2 was not implemented. An experiment was planned in which the robot leg would continuously keep jumping. The phase resistance would be measured between jumps, such that the temperature of the motor could be estimated. However, due to time constraints and some parts breaking this was not possible anymore. The results of this experiment would show if the motor would reach the thermal limit and therefore would require thermal management.

4.2 Jumping Leg

A demo setup has been created in order to make the research relevant for robotics and to test the algorithms on a real setup. This setup consists of a jumping leg that has been constrained to one dimension (see Figure 4.3). A single motor in the hip generates all the power required to make the leg jump. There are no elastic elements in this setup, so it is just raw motor power. A Maxon EC60 Flat motor is used in this setup (see Appendix A). This motor is controlled by the ODrive, an open source motor controller. The specifications of this controller can be found in Appendix B. The firmware on the ODrive has been altered such that both q- and d-axis current references can be sent.

The mass of the leg with the motor block is 2.4 [kg]. The heaviest parts are the motor (0.36 [kg]) and the gearbox (0.77 [kg]). The length of the upper link is 20 [cm] and the length of the lower link is 22 [cm].

This setup is the authors own design. Most parts of the setup are 3D printed. Except for the bearings, shafts, some nuts and bolts and the aluminum frame. Even the larger gears are 3D printed. However, these are 3D printed out of metal. The key in the motor shaft is quite small. An explosive motion requires a lot of force, resulting in the key ripping through the plastic of a 3D printed gear out of PLA. The constructed setup is shown in Figure 4.4.



 $\textbf{Figure 4.3:} \ \ \textbf{The demo application setup as designed in SolidWorks.}$

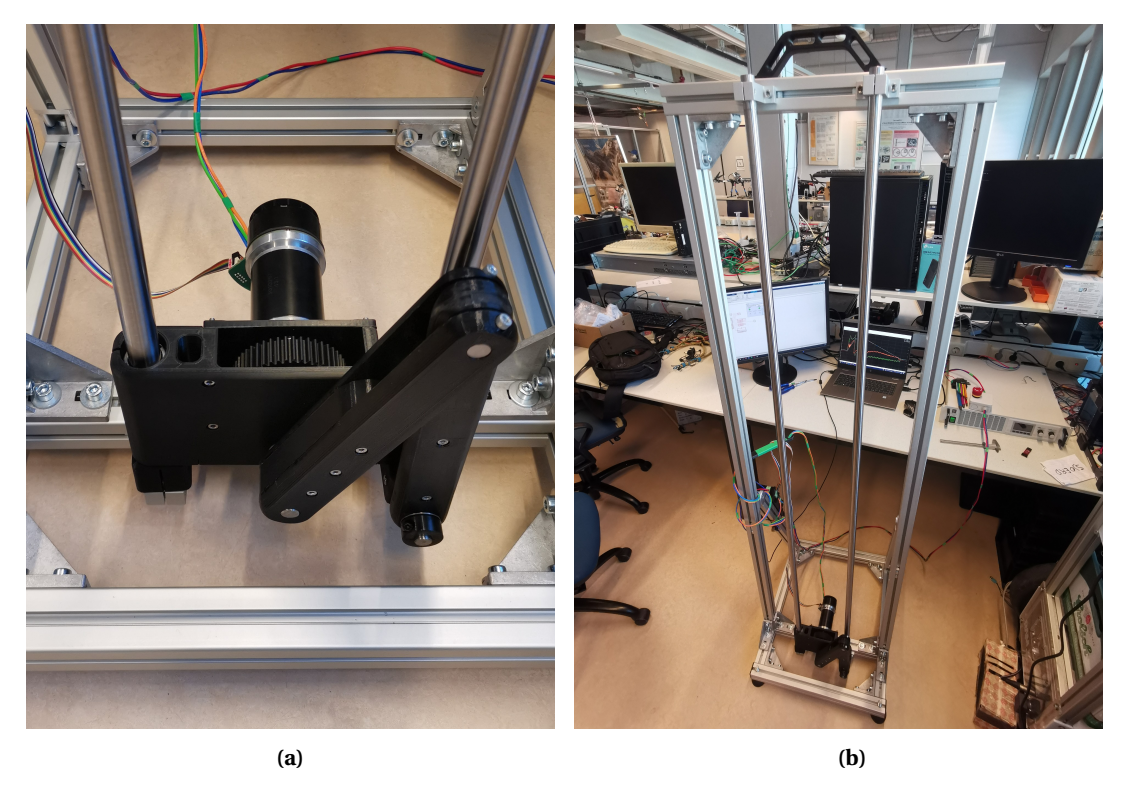


Figure 4.4: The setup.

5 Results

Experiment 1 showcases the strong dependence on the motor parameters by the model based field-weakening controller. Experiment 2 showcases a robotic leg where the jumping performance is evaluated. Two cases are compared: with field-weakening and without.

5.1 Experiment 1: Deviating motor parameters

The goal of this experiment is to evaluate the performance of the field-weakening controller by varying the motor parameters known in the controller compared to the parameters of the actual motor. The motor parameters are varied from -30% to +30% with respect to the actual parameters in the motor model. The motor is accelerated with a constant torque until it reaches a steady velocity.

The SPMSM motor is modelled in Matlab Simulink with a simple mechanical system that contains an inertia and some damping. The following plots are made with the motor parameters as described in Appendix A. A mass is connected to the motor shaft which has ten times the motor inertia. The only damping in the system is that of the motor itself. The requested torque is a constant 0.4 [Nm]. The controller uses the feed-forward field-weakening method that calculates the current setpoints at 1 kHz (see Section 4.2). There is also a 1 ms time delay in the measured speed of the motor, before it arrives at the controller. The requested torque in combination with the total inertia is chosen such that the performance of the field-weakening algorithm becomes clearly visible.

It can clearly be seen in Figure 5.1 that the performance is the best when the motor parameters in the controller are in agreement with the actual motor parameters. Not only does the motor reach its top speed of 5000 [rpm] the fastest, but the top speed itself is also the highest. Furthermore, the results in Figure 5.1 are acquired by only varying one motor parameter. The performance will degrade even more if all parameters are off at the same time.

The winding resistance is subject to change due to a temperature change. It can be seen in Figure 5.1a that the field weakening performance degrades when the motor heats up. For example, if the motor heats up by 50 [°C], the performance of the algorithm matches that of the horizontal level at -20%. A similar top speed of the motor compared to the nominal situation is reached, but it just takes longer to reach it.

The resistance is not the only parameter affected by the temperature change. The k_t parameter is affected as well. The permanent magnets are weakened as the motor heats up. Therefore, the permanent magnet flux, λ_m is lower. The torque constant, k_t , is directly related to the permanent magnet flux. For example, if the motor heats up by 50 [°C], the performance of the algorithm matches that of the horizontal level at +6% in Figure 5.1c as calculated with Equation 3.3. The top speed of the motor is reduced and it also takes much longer to reach this top speed. This is mainly due to the fact that in mode 1 of the field-weakening controller the direct current is set too low. Therefore, the quadrature current cannot be maintained and the torque output of the motor reduces. This in turn results in a slower acceleration of the motor.

Figure 5.1b shows that it is important to accurately measure the phase inductance. Overestimating the inductance by 10% significantly reduces the top speed of the motor. Whereas underestimating the inductance only results in reaching the top speed a bit later.

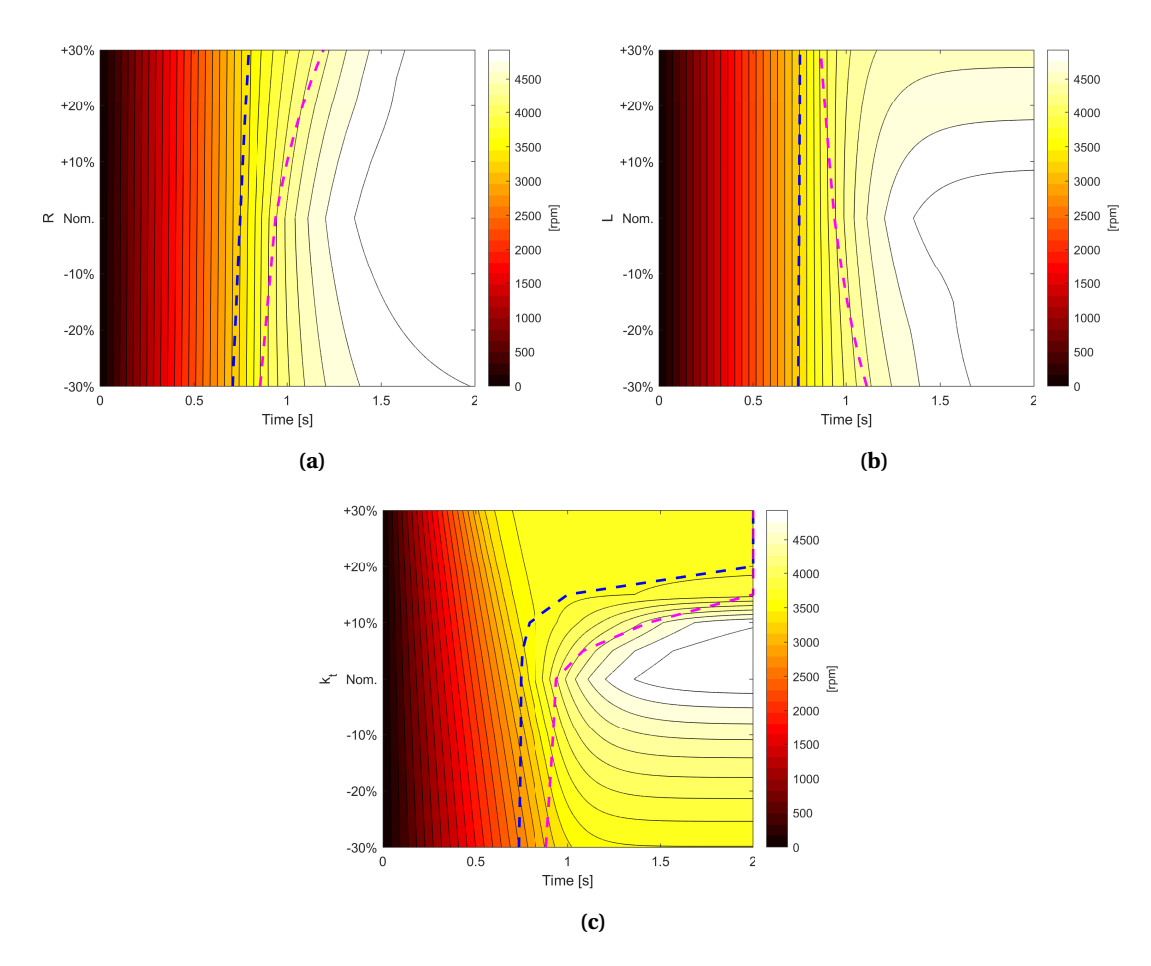


Figure 5.1: Motor speed over two seconds with model based field-weakening for variations of R, L and k_t in the controller. The blue and magenta dashed line indicates the points were field-weakening mode 1 or mode 2 is engaged.

5.2 Experiment 2: Jumping with robotic leg

The goal of this experiment is to test the jumping performance of a robotic leg with and without field-weakening. First, this is done with a mechanical model of the leg in Simulink in Section 5.2.1. Then, it is also tested with the real leg in Section 5.2.2.

The leg has to jump with just a single motor in the hip. Therefore, the leg has to be stretched as fast as possible to launch the leg into the air as high as possible. The motion of the leg is shown in 8 steps in Figure 5.2. The leg is slightly bend during the landing such that a small part of the impact of the landing is absorbed by the motor. The leg should not be bend too much as this would induce a high peak torque in the gearbox. These peak torques could permanently damage the gearbox.

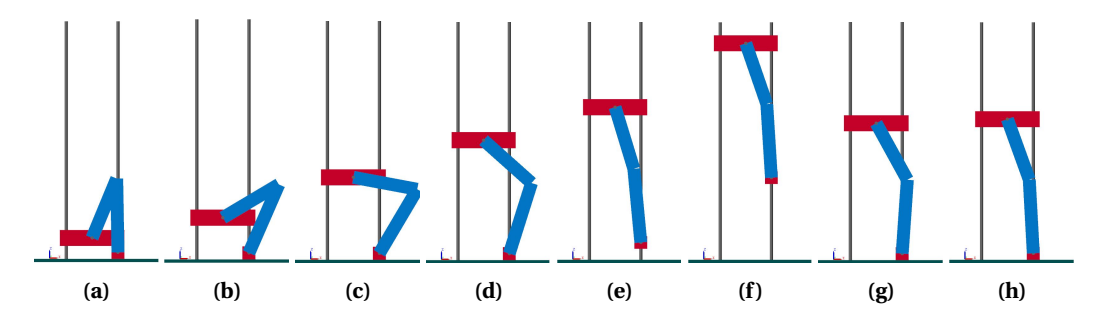


Figure 5.2: The motion of the leg during a jump.

5.2.1 Simulation Results

A simplified mechanical model of the leg is made in Simulink with the toolbox Simscape Multibody. These simulations are used to validate the performance enhancement of the field-weakening strategy and to see how much more the motor will heat up when field-weakening is used.

The position of the leg is controlled by a PD-controller at 1 kHz. The gains of the PD-controller are tuned manually. The position controller generates the torque setpoints based on the error between the reference motor angle and the actual motor angle. The field-weakening controller in turn uses this torque setpoint to calculate the current setpoints also at 1kHz. The weight of both the upper and lower link is 200 grams. The hip block weighs 2 kg and the toe weighs 100 grams. The hip is mainly this heavy due to the motor and gearbox.

The jump is executed as fast as possible. This means that the torque requested at the start of the jump should be as large as possible and therefore also the quadrature current is as large as possible. Hence, the required quadrature current directly hits the current limit circle. Therefore, the field-weakening algorithm directly engages mode 2 while speeding up.

Figure 5.3 shows the simulation results. It can be seen in Figure 5.3a that the i_q current drops to 10 [A] in the case with no field-weakening. With field-weakening the i_q current is also reduced but less. The field-weakening algorithm reduces the i_q in order to stay at the current limit, see Section 3.2.1 mode 2. From this figure it can also be seen that the motion is executed faster as the i_q drops earlier back to zero again for the field weakening case.

The i_d currents are shown in Figure 5.3b. In the non-field-weakening case it can be seen that the i_d current is non-zero. The requested direct and quadrature voltages by the PI controllers in the motor controller cannot be achieved as its magnitude of both these voltages is larger than the voltage limit. Both the direct and quadrature voltages are scaled down in order to satisfy the voltage limit. This is done by the DQ-limiter block in Figure 4.2. This results in some non-zero direct axis current and a reduction of the quadrature current.

It can be seen in Figure 5.3c that the top speed of the motor with field-weakening is higher than without field-weakening. 407 [rad/s] compared to 348 [rad/s] respectively. An increase of 18%. It can also be seen that during the motion the motor slows down. This is due to the particular dynamics of the robot leg. At the start the arm for the gravitational forces acting on the main body is relatively short (see Figure 5.2a). When the knee extends outwards the arm becomes larger (see Figure 5.2c). Therefore, also more torque is required to overcome these gravitational forces. In Figure 5.2c the arm length is at its maximum. From this point on the arm length decreases again and the motor will speed up again. This last bit is important as it mainly determines the jumping height.

The vertical main body speed is shown in Figure 5.3d. The higher this vertical velocity the higher the robot leg will jump. The vertical velocity with field-weakening is only 4% or 0.1 [m/s] higher for the field-weakening case. However, in Figure 5.3e it can be seen that this results in a jump that is 3.4 cm higher. An increase of 16% in jump height.

The temperature of the windings in the motor starts at room temperature (300 [K]). After a single jump the temperature increases 0.64 [K] for the non-field-weakening case. For the field-weakening case it increases up to 0.8 [K]. The additional direct axis current is responsible for the higher winding temperature. This illustrates that a single jump significantly heats up the motor, be it with field-weakening or without.

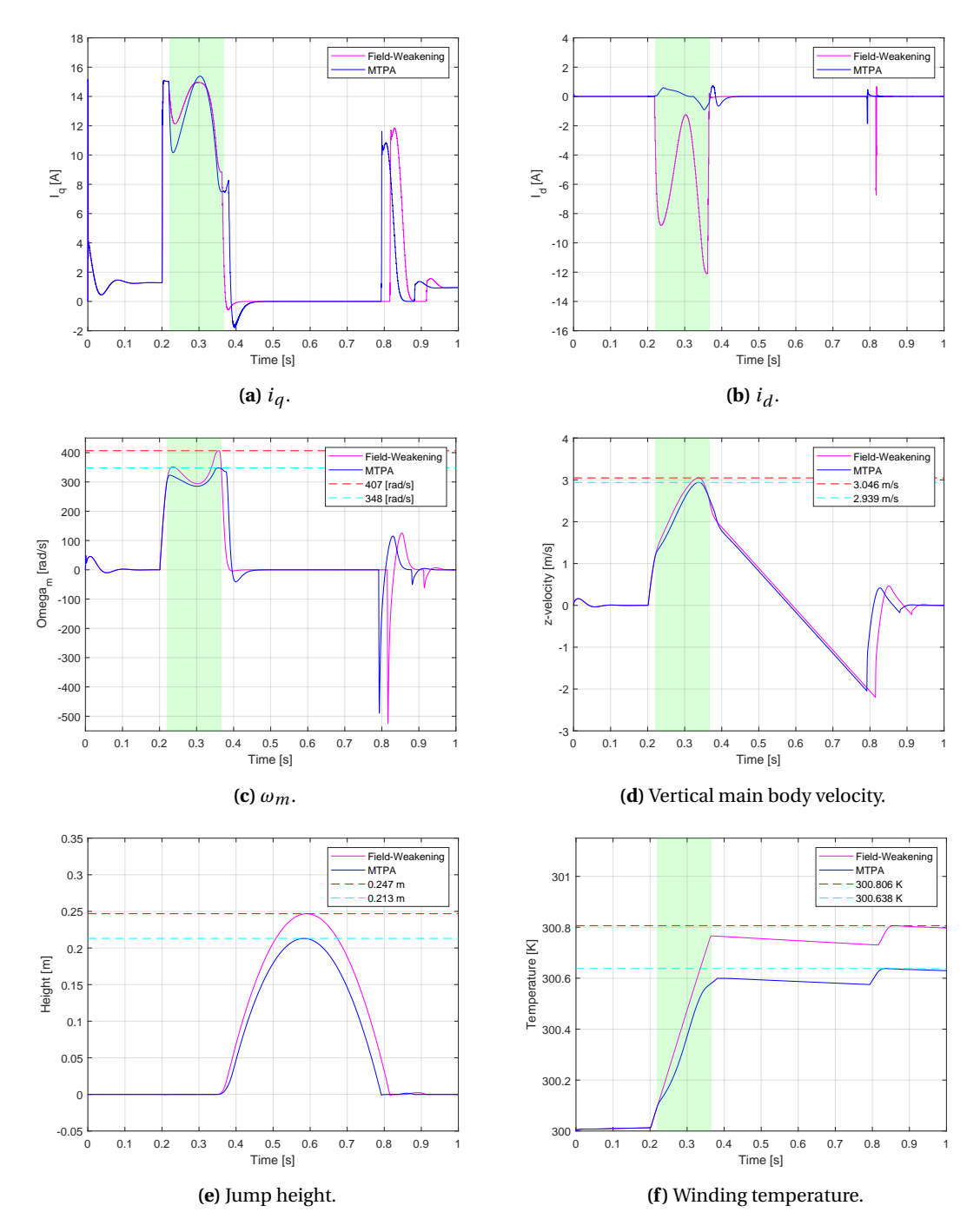


Figure 5.3: Simulation results of jumping with a robotic leg with field-weakening control in magenta and with MTPA control (no field-weakening) in blue. The green areas indicate when field-weakening is used.

5.2.2 Results with Setup

Now the jump is carried out with a real motor in a real setup in order to validate the performance of the field-weakening controller in practice.

The controller part of Figure 4.1 is executed on a real-time kernel provided by Simulink Desktop Real Time. The real-time controller ensures that every 1 ms the current references are send to the ODrive motor controller board. The motor controller board directly sends back the motor position, velocity and measured currents. Hence, the loop delay is 1 ms. The motor angle and

CHAPTER 5. RESULTS 23

angular velocity are used by the controller whereas the currents are only send such that these can be monitored.

The motor controller calibrates the motor before it can jump. During the calibration the motor parameters like phase resistance and phase inductance are measured. These measured values are used in the field-weakening controller.

The goal was to put a temperature sensor directly on the windings in the motor, however this was not possible. Taking the Maxon EC60 Flat motor apart could damage it. Therefore, instead of measuring the temperature directly it is measured indirectly by measuring the winding resistance. Before and after each jump the winding resistance is measured with the ODrive motor board.

A ruler is attached to the aluminum frame in order to measure the jump height. The jumps are recorded by a camera at 60fps. The jump height is determined by slowly scrolling to the captured movie frames and looking at the highest point in the jump.

The current tracking results are shown in Figure 5.4. In the non-field-weakened case it can be seen that the quadrature axis current drops to 10 [A] (see Figure 5.4a). In the field-weakened case the quadrature current drops only to 12.5 [A] (see Figure 5.4b), following the commanded reference current as regulated by mode 2 of the field-weakening algorithm.

The direct axis current in the non-field-weakened case is non-zero. The requested direct and quadrature voltages by the PI_controllers in the motor controller cannot be achieved as the magnitude of both these voltages is larger than the voltage limit. The voltage vector norm is reduced automatically as it simply cannot be generated by the motor controller board. This results in some field-weakened behaviour even with field-weakening control inactive.

Figure 5.4e and 5.4f show the movement in the d-q current plane. In Figure 5.4f it can be seen that the reference current follows the current limit circle to the left. However, the measured quadrature current is slightly lower when the reference moves to the left. This is due to the rapid acceleration of the motor. The direct axis current is not increased fast enough in order to maintain the quadrature current. The opposite is true when the motor slows down again. Then, the measured quadrature current is larger than the current reference as the direct axis current is not reduced fast enough. Furthermore, in Figure 5.4e it can be seen that also without field-weakening active the measured current slightly moves to the left. This is due to the same effect as described in the previous paragraph.

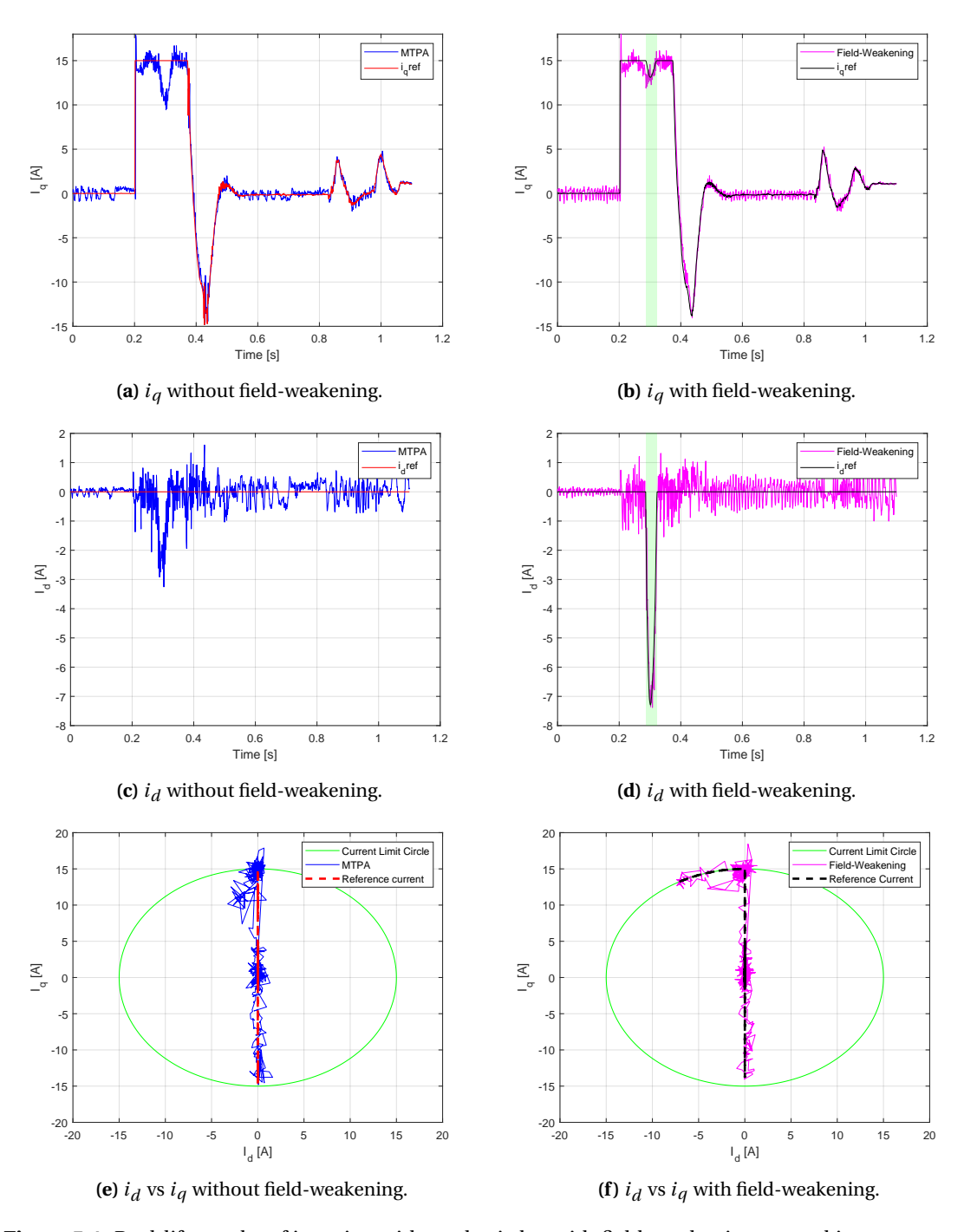


Figure 5.4: Real-life results of jumping with a robotic leg with field-weakening control in magenta and with MTPA control (no field-weakening) in blue. The green areas indicate when field-weakening is used.

CHAPTER 5. RESULTS 25

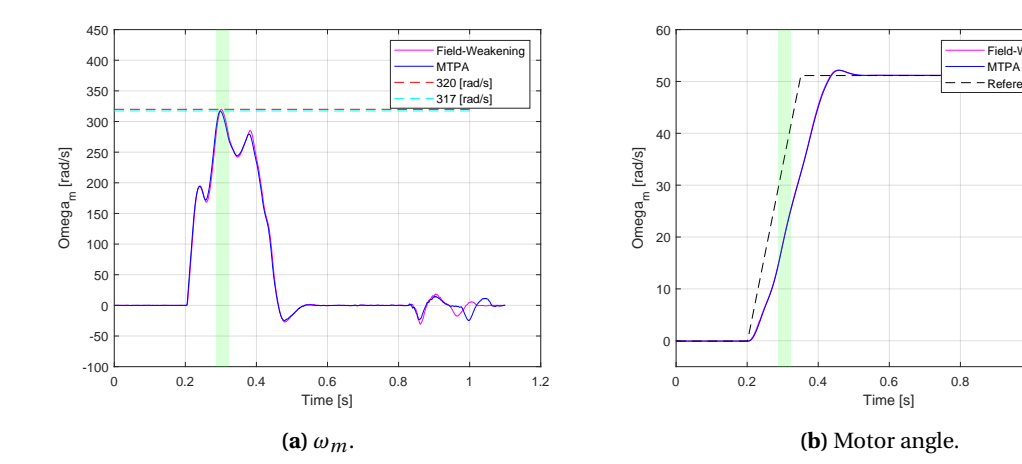


Figure 5.5: Difference in top speed and motor angle. With normal MTPA (without field-weakening) in blue and with field-weakening in magenta.

1.2

The motor velocity and the motor angle are shown in Figure 5.5. The top speed of the motor with field-weakening control is ever slightly higher. 320 [rad/s] compared to the top speed without field-weakening of 317[rad/s]. In Figure 5.5b the measured motor angle position for both cases are quite similar. Also, the resulting jump height of 21.5 [cm] that was captured on camera was the same.

The results with field-weakening active are comparable to the case without field-weakening. However, note that field-weakening is applied for a very short time. Only for 0.035 seconds. The motor accelerates quickly, but decelerates again when the leg stretches further. This behaviour was also seen in the simulation. However, the reduction in motor speed is much more compared to the simulation results in Section 5.2.1. In the second part of the motion from c to e in Figure 5.2 the motor does not reach the field-weakening region anymore. However, the speed in this part is the most important for the jump height.

The resistance measurements before and after jumps to estimate the motor temperature gave inconclusive results. The phase resistance is estimated by applying a current in the direct axis and measuring the voltage for the same axis. The specific rotor angle at which the measurement is done influences the phase resistance. For example, the phase resistance measured at an angle of zero degrees is different from the one at 1 degrees. This difference is in the order of more than ten $m\Omega$'s, which is relatively a large difference if the total measured phase resistance is only 0.22 $[\Omega]$. Measuring the phase resistance at the same rotor angle is not possible as the motor position cannot be controlled during the phase resistance measurement. Therefore, estimating the winding temperature this way might not be the best solution.

Furthermore, the rotor has a fan structure attached to its back. The faster the rotor spins the more air is moved that can cool down the windings. So, the cooling is also the largest during the explosive motion. Therefore, the thermal model is not as simple as it is depicted in Figure 3.4. However, for the thermal management it can still be assumed that no heat will flow to the environment, since the duration of the motion is still much shorter than the thermal time constant of the windings. Mainly, the heat flow from the housing to the environment depends on the rotor speed.

5.3 Discussion

In simulation the jump height is 16% higher for the field-weakened case. In practice the results for the field-weakened case are comparable to the non-field-weakened case. It turned out to be rather difficult to design a jumping leg that can accelerate fast enough for the motor to reach the field-weakening region. Especially, estimating the friction forces in the setup without having the actual setup at hand was hard. They are also highly non-linear due to how the leg is constructed. These parameters can be altered in the simulation model such that it would more closely resemble the actual setup.

The jumping leg that was constructed also was an initial design. Optimizing the gear ratio and the link lengths could improve the jumping performance significantly. Moreover, the motor and gearbox were not selected for this application, but rather where parts that where at hand. This motor had a gearbox attached to it with a ratio of 43:1. This ratio was too high to even jump up. Hence, the ratio had to be reduced again, which is not particularly efficient. It adds inertia to the system and also has more contact surfaces that create frictional losses. The inefficiency of the gearing is probably the main reason why the jumping performance in real-life was not as good as the simulation.

Initially plastic 3D printed gears where used. Due to the lower mass the acceleration of the motor was higher, but these gears were not strong enough to support the large torques required by the explosive motions. The metal 3D printed gears were strong enough for the large torques required, but had their own disadvantages. For instance, they had rough contact surfaces due to the layer by layer deposition process of 3D printing. It was noted that after a large number of jumps the gears teeth surfaces had become smoother and the jumps seemed to be higher. It would have been better to let the gears run for a couple of days in a setup such that the teeth surfaces could become smooth. This would improve the gearing efficiency.

Furthermore, the results in Section 5.2.2 have been acquired with a current limit of 15 [A]. The ODrive motor controller can supply currents up to 120[A], leaving much headroom for more explosive jumping performance. The stall current for the Maxon EC60 Flat motor is specified at 81.9 [A]. This produces the greatest torque in the motor. However, the stall torque as specified in the datasheet is equal to the linearly calculated load torque without magnetic saturation effect (Maxon Motor, 2014). This torque often cannot be achieved due this saturation effect. Hence, pushing more current into the motor will not results into a faster acceleration.

The thermal management strategy as presented in Section 3.3.2 was not implemented. The temperature increase due to an explosive motion depends on a lot of variables. The most important variable is the nominal motor load. For example, if the motor performs the explosive action with a current limit of 15 amperes in 0.2 seconds and takes 5 seconds between jumps. Then, the average current in the motor during this cycle is below 2 amperes, since the current required to lower the leg again to its starting position is only 2 amperes. This is far below the nominal current as specified in the datasheet for the Maxon EC60 Flat motor. Therefore, no thermal management would be required. This would be different for a robot that also has significant motor current between jumps. In that situation the nominal current is much higher and some thermal management might be required.

6 Conclusion and Recommendations

In this thesis existing field-weakening methods for torque controlled actuators where researched. Field-weakening allows a motor to reach higher speeds with a limited supply voltage using existing current reserves. The model-based field-weakening method was determined to be the most robust. The feedback method uses the very noisy commanded voltages and measured currents in the dq-frame. This noise directly enters the PI-controllers creating large current swings in the motor. Filtering these signals could reduce the swings, but make the method less responsive.

The model-based field-weakening method is not without weaknesses. It is strongly dependent on the motor parameters. Imprecise motor parameter identification results in errors in the reference currents generate by the field-weakening controller. Moreover, the motor parameters also change due to temperature changes in the motor. Measuring the motor temperature and correcting the motor parameters accordingly will make the field-weakening algorithm more robust and increase its performance. For instance, a temperature increase of 50°C would significantly reduce the performance due to an increase of 20% in winding resistance and a reduction 6% in the torque constant.

Explosive motions require a lot of power and top speed. Field-weakening increases the top speed, but also requires more power. Therefore, a fatigue management strategy was presented. This would allow a larger current limit when the motor is cold. The limit is reduced the hotter the motor gets. However, due to the short nature of the explosive motion, the nominal current stays below the maximum continuous current. Therefore, for the robot leg that was designed no fatigue management would be required. For other robotic applications where even more current is required during normal operation it might still be a good thermal management strategy.

Finally, the field-weakening performance was evaluated for a jumping leg. Simulation results showed that the jump height increased by 16% when field-weakening is applied. In practice this improvement was not observed. However, the constructed leg is just an initial design. Optimizing the gear ratio and link lengths would definitely improve the jumping and show the value of field-weakening in practice.

In conclusion, field-weakening was applied in an intelligent model-based manner. The improvement of correcting the motor parameters in the field-weakening controller based on the temperature should still be investigated, but it is expected that the model-based field-weakening controller will perform better with this addition.

Abbreviations

FOC Field Oriented Control. 4

IPMSM Interior Permanent-Magnet Synchronous Machine. 10–12

MTPA Maximum Torque Per Ampere. 7, 10–12, 22, 24

PMSM Permanent-Magnet Synchronous Machine. 1–3, 10, 14–16

SPMSM Surface Permanent-Magnet Synchronous Machine. 10–12, 16, 19

A Appendix 1

EC 60 flat Ø60 mm, brushless, 200 Watt

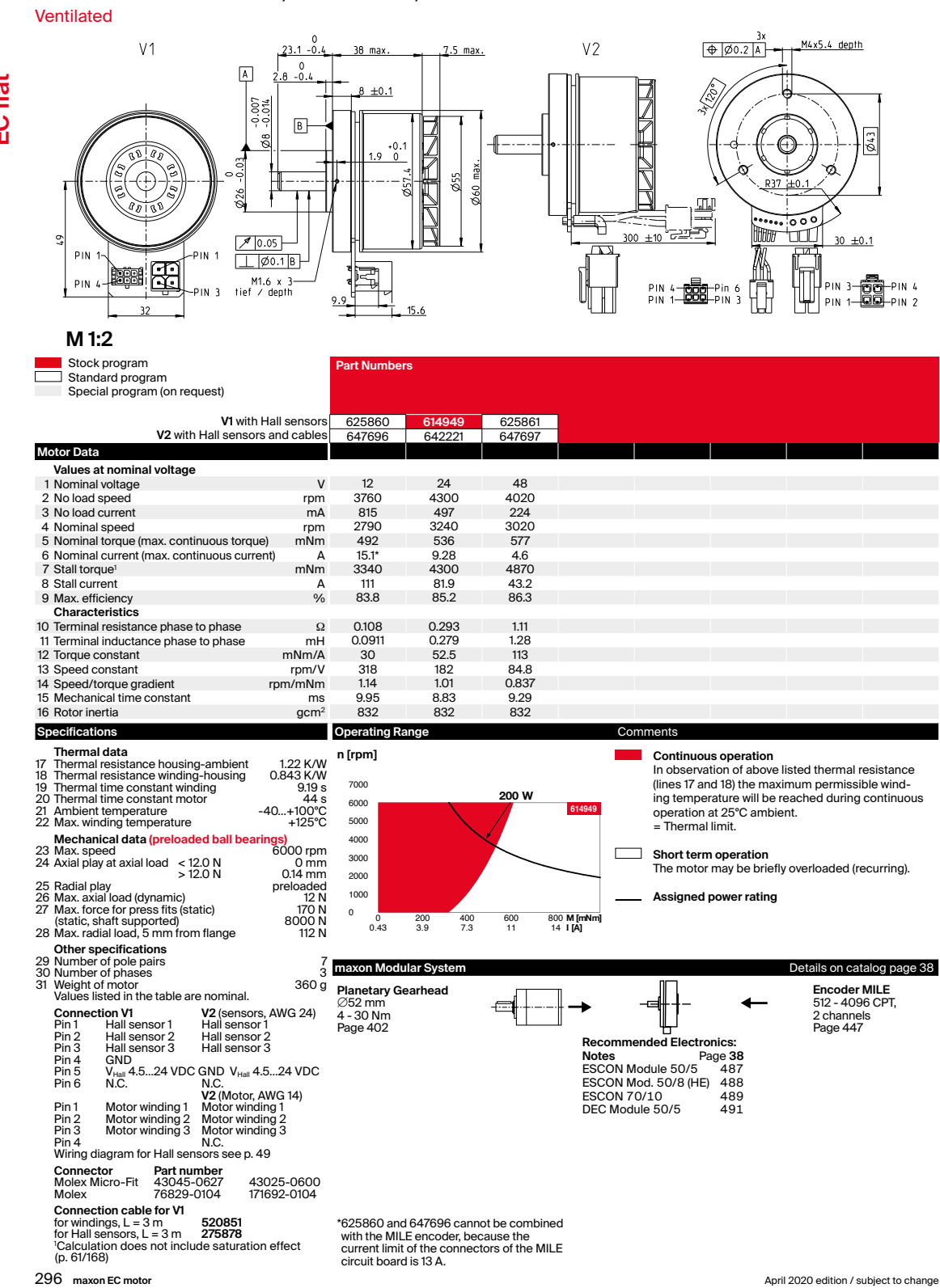


Figure A.1: EC60 flat Maxon motor (614649).

B Appendix 2

The Odrive V3.6 is an open source motor controller board that is capable of controlling two motors. It is supplied with a voltage of 12V to 56V and is capable of delivering a peak current of 120A per motor. The amount of continuous current depends on the cooling. Without active cooling the maximum current is 40A. With the addition of fans the maximum current is 80A. Out of the box it supports: position, velocity and current control. The references for the control loops can be send over USB, UART, CAN or by sending a PWM signal to one of its gpio pins. The interfaces are fast enough to have a control loop off board updating the reference at a rate of 1 kHz.

The current control loop on the board itself runs at 8 kHz. Out of the box it is not possible to send i_d and i_q current commands. This has been implemented by the author.

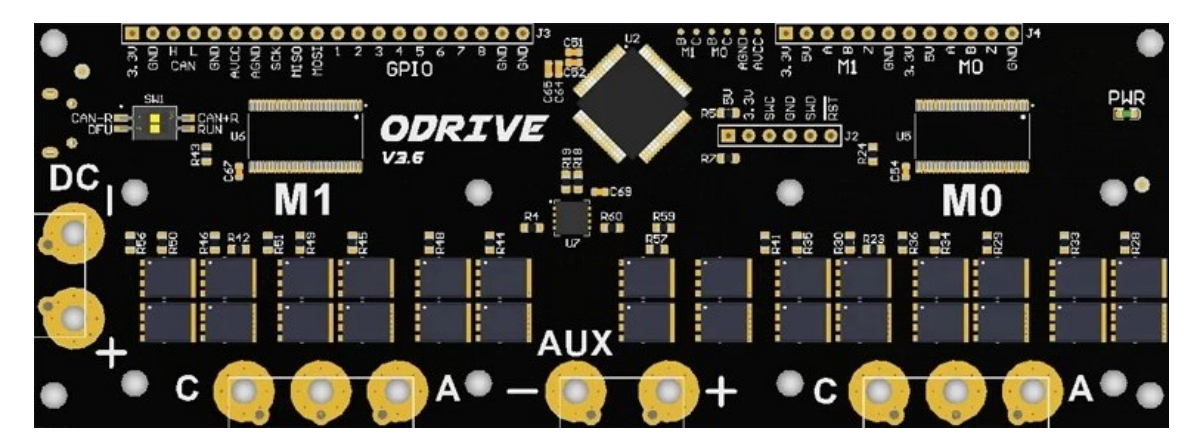


Figure B.1: The ODrive, an open source motor controller.

Bibliography

Breedveld, P. (2001), Integrated Modelling of Physical Systems, 2018 edition.

Maxon Motor (2014), Maxon EC motor iron-cored winding technology – Short and to the point. Maxon Motor (2021), Maxon DC motor and Maxon EC motor - Key information.

Mohammadnia, M., N. Kashiri, F. Braghin and N. G. Tsagarakis (2019), Flux Regulation for Torque-controlled Robotics Actuators, in *2019 19th International Conference on Advanced Robotics (ICAR)*, IEEE, pp. 93–98, ISBN 978-1-7281-2467-4, ISSN 0019-1035, doi:10.1109/ICAR46387.2019.8981613.

https://ieeexplore.ieee.org/document/8981613/

Montone, D. (2020), Temperature Effects on Motor Performance.

Roozing, W., N. Kashiri and N. G. Tsagarakis (2018), Enhanced Explosive Motion for Torque Controlled Actuators Through Field Weakening Control, in *2018 IEEE/RSJ International Conference on Intelligent Robots and Systems (IROS)*, IEEE, February 2019, pp. 1–8, ISBN 978-1-5386-8094-0, ISSN 21530866, doi:10.1109/IROS.2018.8593608.

https://ieeexplore.ieee.org/document/8593608/

Sue, S. M. and C. T. Pan (2008), Voltage-constraint-tracking-based field-weakening control of IPM synchronous motor drives, *IEEE Transactions on Industrial Electronics*, **vol. 55**, pp. 340–347, ISSN 02780046, doi:10.1109/TIE.2007.909087.

http://ieeexplore.ieee.org/document/4401187/